

Demographic controls of future global fire risk

W. Knorr^{1*}, A. Arneth² and L. Jiang^{3,4}

Wildfires are an important component of terrestrial ecosystem ecology but also a major natural hazard to societies, and their frequency and spatial distribution must be better understood¹. At a given location, risk from wildfire is associated with the annual fraction of burned area, which is expected to increase in response to climate warming^{1–3}. Until recently, however, only a few global studies of future fire have considered the effects of other important global environmental change factors such as atmospheric CO₂ levels and human activities, and how these influence fires in different regions^{4,5}. Here, we contrast the impact of climate change and increasing atmospheric CO₂ content on burned area with that of demographic dynamics, using ensembles of climate simulations combined with historical and projected population changes under different socio-economic development pathways for 1901–2100. Historically, humans notably suppressed wildfires. For future scenarios, global burned area will continue to decline under a moderate emissions scenario, except for low population growth and fast urbanization, but start to increase again from around mid-century under high greenhouse gas emissions. Contrary to common perception, we find that human exposure to wildfires increases in the future mainly owing to projected population growth in areas with frequent wildfires, rather than by a general increase in burned area.

Episodic wildfires are a fundamental component of terrestrial ecology¹, and vegetation structure, species composition and natural fire regimes have co-evolved^{1,6}. However, fires also emit large amounts of atmospheric pollutants⁷, damage properties and lives^{1,8}, and complicate climate mitigation efforts such as reforestation and forest conservation⁹. Wildfires thus are often seen as a risk to human societies, and understanding how fire patterns might change in the future is paramount to diverse questions ranging from health to adaptation of fire management strategies and urban development, to climate policy.

Wildfires need a source of ignition, dry, combustible material and favourable weather conditions to spread. Accordingly, multiple studies predict indices of climatic fire risk and fire activity to increase in a future, warmer and often drier world^{2–4}. However, climate change and increasing levels of atmospheric CO₂ affect plant growth and competition, leading to changes in ecosystem structure and associated flammability, which need to be accounted for when investigating fire in a future environment. Increasing presence of humans leads not only to more ignitions, but humans also actively suppress fire by changing vegetation, removing fuel, and through landscape fragmentation¹⁰. Observation-based studies conducted at the continental to global scale have shown that the impact of increasing human-population density on burned area is generally negative^{11–15}. This study focuses on burned area as opposed to number of fires, because it is the former that is directly related to the

probability of fire¹⁴ and thus is a better indicator of risk to human societies through loss of properties and lives, as well as emission-related health effects.

We use the semi-empirical simple fire model¹⁴ (SIMFIRE), coupled with the global dynamic vegetation model LPJ-GUESS¹⁶. SIMFIRE parameters are derived directly at the global scale using several years of global satellite data of burned area and vegetation structure, combined with climate observations and demographical data (see Methods). We consider the impacts of demographic trends by adopting the population¹⁷ and urbanization¹⁸ projections from the new socio-economic scenario framework for climate change research—the shared socio-economic pathways¹⁹ (SSPs, Table 1). The five SSPs are described through qualitative narratives and quantitative projections of the key elements including changes in population and urbanization, under which the world faces different levels of challenges to climate change mitigation and adaptation. We can thus address not only how fire frequency (fractional burned area) and risk will change in response to climate change, but also how interactions between climate, CO₂, vegetation structure and human interference modify and shape the climatic response.

Depending on the factors taken into consideration, simulated total burned area ranges from 3.0 to 3.8 million km² yr⁻¹ at the beginning of the simulations (Fig. 1). Neither climate change nor increasing levels of atmospheric CO₂ introduce a historical trend in fire frequency over the past century. Instead, the main driver of change is increasing population density, leading to declining burned area as previously shown with a stand-alone version of SIMFIRE¹⁴. Proxy records from charcoal²⁰ and Antarctic ice cores²¹ and recent observed trends²² support the result. These do come with some caveats²³, in particular in recent decades in which some regions seemingly show opposing trends²⁴. Yet, as discussed in ref. 24, these conflicting observations are to be expected as a result of decadal-scale climate variability and the limited length of the satellite record. Furthermore, the authors attribute the strong downward trend in Northern Hemisphere Africa to changing land use and conclude that we are likely to see a secular decline in burned area in all of Africa, as predicted by the present study. Previous global simulations for the twentieth century that accounted for climate, vegetation and human-population effects also resulted in declining fire activity during most of the twentieth century^{4,5}.

In contrast to the historical changes, the projected burned area driven by climate change alone has a clear upward trend over the twenty-first century for the two Earth system model (ESM) ensemble means based on the Representative Concentration Pathways²⁵ (RCPs) 4.5 and 8.5, respectively. However, when adding effects of atmospheric CO₂, projected increases are greatly reduced, with simulated burned area at the end of the twenty-first century being near or only slightly above present-day levels. This result seemingly

¹Department of Physical Geography and Ecosystem Science, Lund University, Sölvegatan 12, 223 62 Lund, Sweden. ²Division of Ecosystem-Atmosphere Interactions, Karlsruhe Institute of Technology, Institute of Meteorology and Climate Research/Atmospheric Environmental Research, Kreuzeckbahn Str. 19, 82467 Garmisch-Partenkirchen, Germany. ³Asian Demographic Research Institute, School of Sociology and Political Science Shanghai University, 99 Shangda Road, Shanghai 200444, China. ⁴National Center for Atmospheric Research, PO Box 3000, Boulder, Colorado 80307-3000, USA.

*e-mail: wolfgang.knorr@nateko.lu.se

Table 1 | Historical and future measures of fire risk to humans.

Scenario		Case	Global pop. (10 ⁹) [†]		Regions with >30 people km ⁻² ‡						Fire-prone regions ^{§§}		
Population	Urbanization		Population (10 ⁹) [†]	Area (10 ⁶ km ²)	Fire freq. (10 ⁻³ yr ⁻¹)		Total burned area (10 ³ km ² yr ⁻¹)		Grass fraction		Total people (10 ⁶)		
					RCP4.5	RCP8.5	RCP4.5	RCP8.5	RCP4.5	RCP8.5	RCP4.5	RCP8.5	
Historical period 1971–2000*		0	4.9	4.4	15.2	11.0		168		23%		413	
SSP5 (low)	SSP5 (fast)	1	7.8	7.5	17.6	9.1	9.0	160	158	20%	17%	508	527
SSP2 (medium)	SSP5 (fast)	2	9.4	9.1	19.4	9.9	9.8	192	191	20%	17%	497	538
SSP2 (medium)	SSP2 (medium)	3	9.4	9.1	22.2	10.5	10.4	232	231	21%	17%	560	610
SSP2 (medium)	SSP3 (slow)	4	9.5	9.1	25.5	10.9	10.9	278	277	21%	17%	622	673
SSP3 (high)	SSP3 (slow)	5	12.4	12.1	28.0	10.4	10.2	291	286	21%	17%	646	716
Difference between scenarios													
Change of SSP5 to SSP2 pop.		2–1	1.6	1.6	1.8	0.8	0.8	32	33	0%	0%	–11	11
Change of SSP5 to SSP2 urb.		3–2	0	0	2.8	0.6	0.6	40	40	1%	0%	63	72
Change of SSP2 to SSP3 urb.		4–3	0	0	3.3	0.4	0.5	46	46	0%	0%	62	63
Change of SSP2 to SSP3 pop.		5–4	2.9	3.0	2.5	–0.5	–0.7	13	9	0%	0%	24	43

pop., population; urb., urbanization. *SSP scenarios 2071–2100. [†]Average over the corresponding time period. [‡]Analysis excludes areas with >50% croplands. ^{§§}With fire frequency of 0.01 per year or higher.

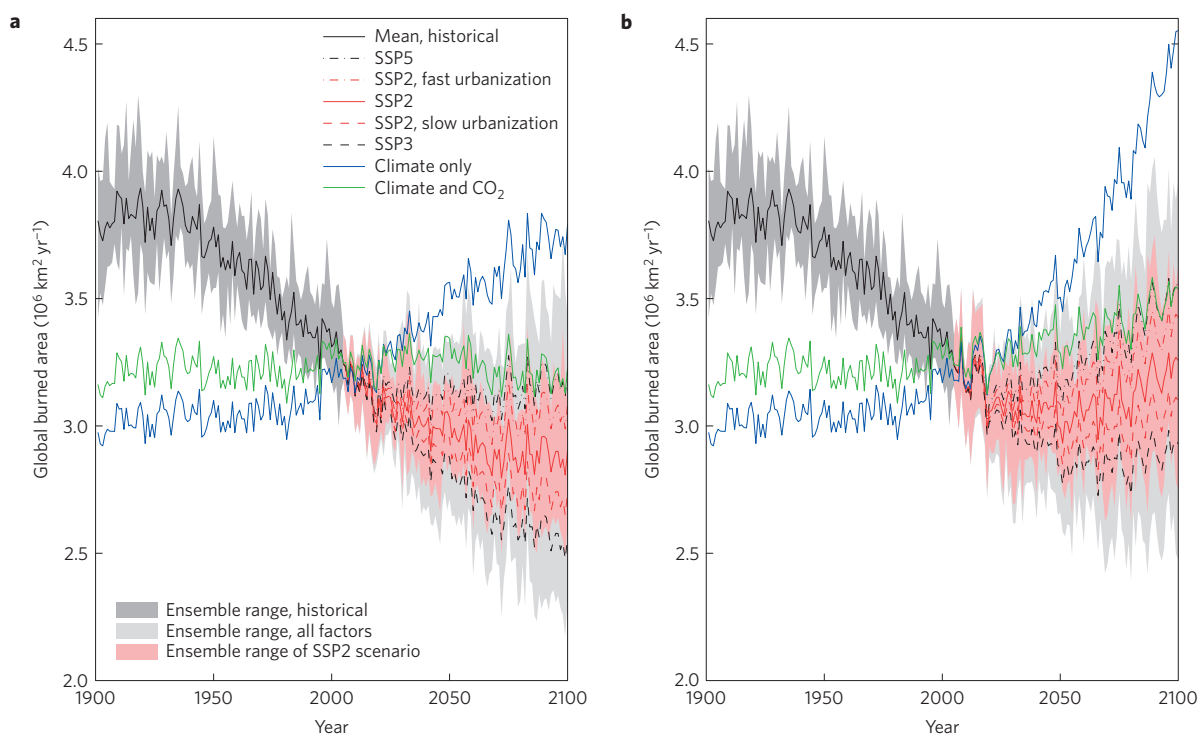


Figure 1 | Eight-ESM ensemble means of simulated global burned area based on varying climate alone, varying climate and CO₂ alone, and for all factors including population density. The eight-ESM ensemble range is shown for the central SSP2 population scenario (red) or the historical period (dark grey), and for the full ensemble range of eight ESMs and five different population scenarios (light grey). **a**, RCP4.5 emissions. **b**, RCP8.5 emissions.

contradicts the expected CO₂-fertilization response, because enhanced vegetation net primary production would also lead to denser vegetation²⁶, and therefore to a more continuous fuel bed, enhancing fire spread. However, enhanced levels of CO₂ favour plants of the C3 photosynthesis type causing these to operate at more efficient rates of carboxylation²⁷. Consequently, shrub encroachment is simulated to occur in the savannah biome, similar to what has been observed at a number of sites and regions already^{28–30} (see Supplementary Fig. 1). As >70% of the total global burned area is found in savannahs²², caused by rapid spread of grassland fires, the reduced fire spread as shrubs become more dominant at the expense of grass cover (see equation (1) and Supplementary Table 2) becomes quickly visible in global burned-area numbers.

When climate and CO₂ changes are combined with medium population and central urbanization trends under SSP2, future fire frequency is projected either to decline until the late twenty-first century (RCP4.5), or to return to approximately current levels (RCP8.5). Even though Asia and other parts of the developing world also show strong differentiation of predicted burned area by urbanization scenario (Supplementary Table 3 and Supplementary Fig. 2), the declining trend is dominated by the African continent (Supplementary Fig. 2), largely because, at present, Africa accounts for about half the global burned area²² and has the most fundamental projected demographic changes¹⁹. These findings differ from previous work accounting for the combined climate, vegetation and human factors, which suggested that future fire activity⁴

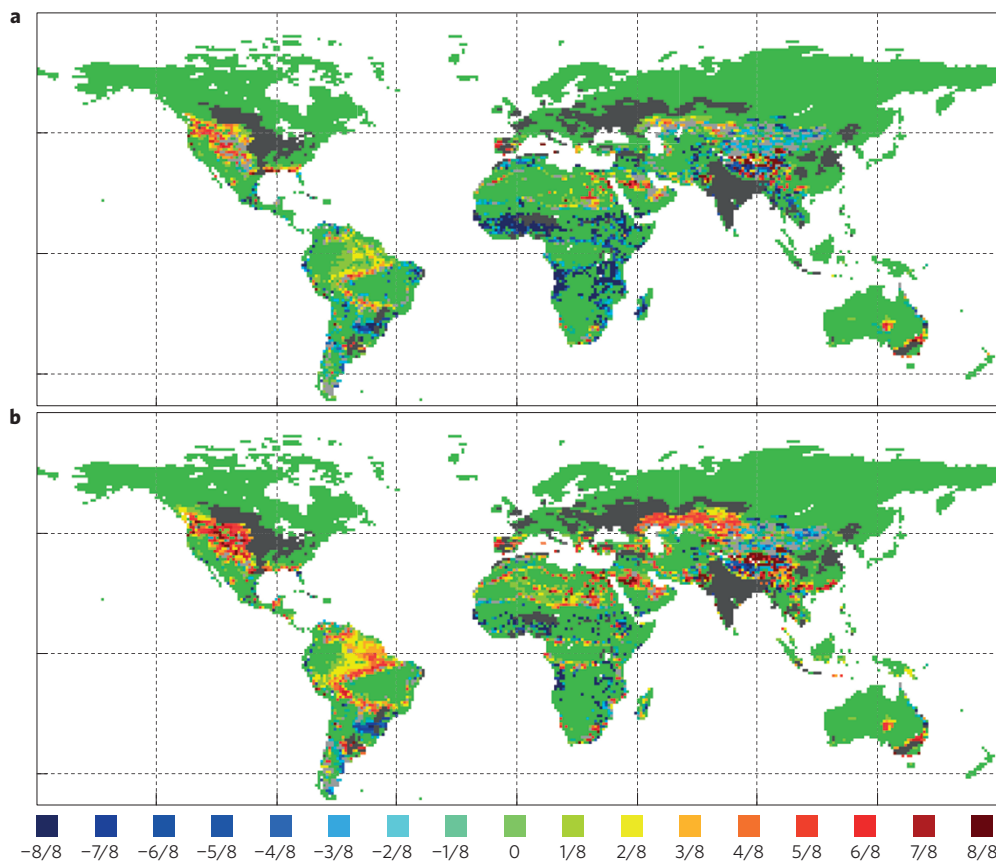


Figure 2 | The probability of low-fire regions becoming fire prone (positive values), or of fire-prone areas changing to a low-fire state (negative values) between 1971–2000 and 2071–2100 based on eight-ESM ensembles. Light grey: areas where at least one ensemble simulation predicts a positive and one a negative change (lack of agreement). Dark grey: areas with >50% past or future cropland. Fire-prone areas are defined as having a fire frequency of $>0.01 \text{ yr}^{-1}$. **a**, RCP4.5 emissions with SSP3 demographics. **b**, RCP8.5 emissions with SSP5 demographics.

or emissions from wildfires⁵ will be significantly higher than at present—even though in these studies projections with all factors combined were also lower than those based solely on climate change. Our study, taking into account both changes in population size and in its spatial distribution due to urbanization, identifies widely varying effects of human activities on future fire regimes.

To demonstrate the importance of urbanization and spatial population patterns, we conduct several sensitivity analyses using different combinations of urbanization and population growth scenarios (Fig. 1). We find that changing only the rate of urbanization (from the central SSP2 to the fast SSP5 scenario, using the same SSP2 medium population growth) increases future (2071–2100) global burned area by about half as much as changing both population and urbanization from SSP2 (medium population growth, central urbanization) to SSP5 (low population growth and fast urbanization). This applies to both RCPs and across all ESMs (Supplementary Table 4). Conversely, slow instead of central urbanization under the same SSP2 medium population scenario reduces future burned area by about half as much as changing both urbanization and population from SSP2 to SSP3.

Newly emerging fire-prone areas (fire frequency $>0.01 \text{ yr}^{-1}$, the upper range of observed fire frequency in the Mediterranean²²) or areas ceasing to be fire prone are shown in Fig. 2 for RC8.5/SSP5 and RCP4.5/SSP3, the two combinations with the highest and lowest global burned area. The regions where climate change leads to an increase and the regions where demographic changes lead to a decrease in fire risk seem to be geographically distinct. For instance, a reduction in fire risk is simulated mainly for many regions in Africa, the continent with the largest burned area at present²². These

are regions that expect moderate to large increases in population density (see Supplementary Figs 3–5), albeit with large differences between SSP3 and SSP5, and, at present, contain large expanses of grasslands. An expansion of fire-prone areas into the Amazon rainforest and the moist savannahs and woodlands to the south is driven by increases in climatic fire risk (Supplementary Figs 6 and 7), as are increases in fire risk for the North American plains or southern Europe.

To normalize results for the effects of changing demography and vegetation structure, we show averages over regions of defined ranges of population density and grass fraction of vegetation (herbaceous divided by total herbaceous and woody, Fig. 3). Fire frequency decreases towards low fractions of grasses and also from intermediate population density towards the most densely populated category, consistent with equation (1). However, there is also a decrease towards zero population density and a maximum mostly in the range of 1 to 10 people km^{-2} (see ref. 15). For the future scenarios, we find a consistent increase in fire frequency for the most sparsely populated category, which is much more pronounced for RCP8.5/SSP5 than for RCP4.5/SSP3, in accordance with the expected impact of climate change. However, changes in fire frequency and burned area in Fig. 3 also reflect changes in the geographic range of specific population and grass fraction categories. The most highly fire-prone areas in Africa decrease their grass fraction from values typically above 0.8 to values often below 0.6 owing to shrub encroachment (Supplementary Fig. 1). As a result, fire frequency increases most strongly in the intermediate grass fraction range. Burned area is shifted generally towards regions with lower population density and away from regions with high

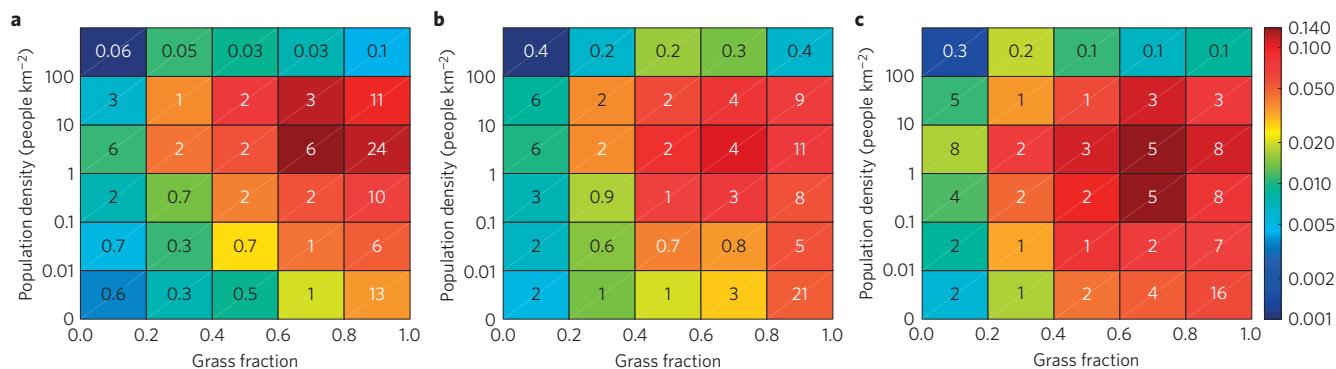


Figure 3 | Two-dimensional histogram plots showing mean fire frequency (fractional burned area, colour scale, in yr^{-1}) and fraction of global burned area (%) by ranges of grass fraction of total (grass and woody) vegetation and population density. **a**, Burned area, population and grass fraction for 1971–2000. **b,c**, Burned area, population and grass fraction for 2071–2100; RCP4.5 emissions with SSP3 demographics (**b**) and RCP8.5 emissions with SSP3 demographics (**c**).

grass fraction. Most of the global reduction in burned area can be attributed to regions with >0.8 grass fraction (see Supplementary Fig. 8). There is also a marked increase in the total burned area for areas with >30 people km^{-2} (Table 1) due to the spread of humans into fire-prone areas, mainly in Africa (Supplementary Fig. 5).

During 1971–2000, 91% of the world population were living in areas with at least 30 people per km^2 , which is also an approximate minimum population density for the wildland–urban interface³¹. This fraction is projected to increase to between 96% (SSP5) and 97% (SSP3) towards the end of the century, whereas the corresponding area would increase moderately for SSP5 and almost double for SSP3 (Table 1 and Supplementary Fig. 5). At the same time, we find that fire frequency in these areas is projected to slightly decline, most strongly under the low population growth/fast urbanization scenario of SSP5. At a given SSP, the decrease is even slightly larger under RCP8.5 than RCP4.5, which can be attributed to a lower grass fraction for RCP8.5 due to higher levels of atmospheric CO_2 . Even though fire frequency declines moderately in densely populated areas, this decline is more than compensated with respect to total burned area owing to the large increase of land area with high population density. As a result, total burned area in highly populated areas increases in all scenarios but SSP5, with a 70% increase for SSP3. Different degrees of future urbanization can lead to large differences (of more than 120 million) between the number of people living in fire-prone areas even when the overall population per country remains the same, independent of the climate scenario. For both measures of fire risk to humans—total burned area in populated areas and population in fire-prone regions—changing the rate of population growth has a markedly smaller effect than changing the rate of urbanization (Table 1). It thus seems that future increases in wildfire risk are determined mainly by an increase of the areal extent of rural and semi-urban population³¹, and not by an increase in fire frequency, especially in the developing world outside of sub-Saharan Africa (see Supplementary Table 3). Moreover, changes in urban forms such as transitions from compact cities to urban sprawl may generate larger impacts on future wildfire risks and warrant further research.

These findings provide useful information for assessing and mitigating the impacts of fire risks on human societies. Fire effects are expected to be largest in scenarios where urbanization is slow, and there is a rapid growth in rural population or an expansion of the wildland–urban interface³¹ where losses of assets are expected to be largest⁸. Potential new fire-prone regions are the north American and central Asian steppes, southern Europe and central South America, with much higher probability under RCP8.5 than under RCP4.5. Even though the spatial scale of our model is relatively coarse, we show here that future urbanization

trends are more important for predicting future exposure to fire risk than changes in population numbers, and that rapid urbanization could become the main driver leading to a rebound in fire activity following a steady decline during the past century. The result is robust against large variations in the assumed population growth, degree of urbanization, CO_2 emissions pathways and changes in model parameterization (see Supplementary Table 5). We find that the world is likely to have to cope with increasing wildfire threats to societies, and future fire management should account for uncertainties in future population change as well as climate and vegetation shift.

Methods

Methods and any associated references are available in the [online version of the paper](#).

Received 17 June 2015; accepted 21 March 2016;

published online 2 May 2016; corrected online 9 May 2016

References

- Bowman, D. M. J. S. *et al.* Fire in the Earth system. *Science* **324**, 481–484 (2009).
- Flannigan, M. D., Krawchuk, M. A., de Groot, W. J., Wotton, B. M. & Gowman, L. M. Implications of changing climate for global wildland fire. *Int. J. Wildland Fire* **18**, 483–507 (2009).
- Krawchuk, M. A., Moritz, M. A., Parisien, M. A., Van Dorn, J. & Hayhoe, K. Global pyrogeography: the current and future distribution of wildfire. *PLoS ONE* **4**, e502 (2009).
- Pechony, O. & Shindell, D. T. Driving forces of global wildfires over the past millennium and the forthcoming century. *Proc. Natl Acad. Sci. USA* **107**, 19167–19170 (2010).
- Kloster, S. *et al.* Fire dynamics during the 20th century simulated by the Community Land Model. *Biogeosciences* **7**, 1877–1902 (2010).
- Running, S. W. Ecosystem disturbance, carbon, and climate. *Science* **321**, 652–653 (2008).
- Kasischke, E. S. & Penner, J. E. Improving global estimates of atmospheric emissions from biomass burning. *J. Geophys. Res.* **109**, D14S01 (2004).
- Moritz, M. A. *et al.* Learning to coexist with wildfire. *Nature* **515**, 58–66 (2014).
- Böttcher, H., Kurz, W. A. & Freibauer, A. Accounting of forest carbon sinks and sources under a future climate protocol—factoring out past disturbance and management effects on age-class structure. *Environ. Sci. Policy* **11**, 669–686 (2008).
- Guyette, R. P., Muzika, R. M. & Dey, D. C. Dynamics of an anthropogenic fire regime. *Ecosystems* **5**, 472–486 (2002).
- Archibald, S., Roy, D. P., van Wilgen, B. W. & Scholes, R. J. What limits fire? An examination of drivers of burnt area in Southern Africa. *Glob. Change Biol.* **15**, 613–630 (2009).
- Archibald, S., Scholes, R. J., Roy, D. P., Roberts, G. & Boschetti, L. Southern African fire regimes as revealed by remote sensing. *Int. J. Wildland Fire* **19**, 861–878 (2010).
- Lehsten, V., Harmand, P., Palumbo, I. & Arneith, A. Modelling burned area in Africa. *Biogeosciences* **7**, 3199–3214 (2010).

14. Knorr, W., Kaminski, T., Arneith, A. & Weber, U. Impact of human population density on fire frequency at the global scale. *Biogeosciences* **11**, 1085–1102 (2014).
15. Bistinas, I., Harrison, D. E., Prentice, I. C. & Pereira, J. M. C. Causal relationships vs. emergent patterns in the global controls of fire frequency. *Biogeosciences* **11**, 5087–5101 (2014).
16. Ahlström, A., Schurgers, G., Arneith, A. & Smith, B. Robustness and uncertainty in terrestrial ecosystem carbon response to CMIP5 climate change projections. *Environ. Res. Lett.* **7**, 044008 (2012).
17. KC, S. & Lutz, W. The human core of the shared socioeconomic pathways: population scenarios by age, sex and level of education for all countries to 2100. *Glob. Environ. Change* <http://dx.doi.org/10.1016/j.gloenvcha.2014.06.004> (2014).
18. Jiang, L. & O'Neill, B. C. Global urbanization projections for the Shared Socioeconomic Pathways. *Glob. Environ. Change* <http://dx.doi.org/10.1016/j.gloenvcha.2015.03.008> (2015).
19. Jiang, L. Internal consistency of demographic assumptions in the shared socioeconomic pathways. *Popul. Environ.* **35**, 261–285 (2014).
20. Marlon, J. R. *et al.* Climate and human influences on global biomass burning over the past two millennia. *Nature Geosci.* **1**, 697–702 (2008).
21. Wang, Z., Chappellaz, J., Park, K. & Mak, J. E. Large variations in Southern Hemisphere biomass burning during the last 650 years. *Science* **330**, 1663–1666 (2010).
22. Giglio, L., Randerson, J. T. & van der Werf, G. R. Analysis of daily, monthly, and annual burned area using the fourth-generation global fire emissions database (GFED4). *J. Geophys. Res.* **118**, 317–328 (2013).
23. van der Werf, G. R., Peters, W., van Leeuwen, T. T. & Giglio, L. What could have caused pre-industrial biomass burning emissions to exceed current rates? *Clim. Past* **9**, 289–306 (2013).
24. Andela, N. & van der Werf, G. R. Recent trends in African fires driven by cropland expansion and El Niño to La Niña transition. *Nature Clim. Change* **4**, 791–795 (2014).
25. Moss, H. R. *et al.* The next generation of scenarios for climate change research and assessment. *Nature* **463**, 747–756 (2010).
26. Donohue, R. J., Roderick, M. L., McVicar, T. R. & Farquhar, G. D. Impact of CO₂ fertilization on maximum foliage cover across the globe's warm, arid environments. *Geophys. Res. Lett.* **40**, 3031–3035 (2013).
27. Long, S. P., Osborne, C. P. & Humphries, S. W. in *Global Change: Effects on Coniferous Forests and Grasslands* (eds Breymer, A. I., Hall, D. O., Melillo, J. M. & Ågren, G. I.) 121–181 (Wiley, 1996).
28. Morgan, J. A., Milchunas, D. G., LeCain, D. R., West, M. & Mosier, A. R. Carbon dioxide enrichment alters plant community structure and accelerates shrub growth in the shortgrass steppe. *Proc. Natl Acad. Sci. USA* **104**, 14724–14729 (2007).
29. Wigley, B. J., Bond, W. J. & Hoffman, M. T. Thicket expansion in a South African savanna under divergent land use: local vs. global drivers? *Glob. Change Biol.* **16**, 964–976 (2010).
30. Buitenwerf, R., Bond, W. J., Stevens, N. & Trollope, W. S. W. Increased tree densities in South African savannas: > 50 years of data suggests CO₂ as a driver. *Glob. Change Biol.* **18**, 675–684 (2012).
31. Syphard, A. D. *et al.* Human influence on California fire regimes. *Ecol. Appl.* **17**, 1388–1402 (2007).

Acknowledgements

A.A. and W.K. acknowledge support from the EU FP7 projects PEGASOS (265148) and LUC4C (603542). A.A. also acknowledges support from the Helmholtz Association in the ATMO programme and through its Innovation and Networking fund. W.K. thanks A. Ahlström for providing gridded driving data from the CMIP5 simulations.

Author contributions

W.K. and A.A. conceived the study, L.J. provided the population scenarios, and W.K. performed simulations and numerical analyses. W.K. and A.A. wrote the first draft of the manuscript. All authors contributed to discussion of results and writing.

Additional information

Supplementary information is available in the online version of the paper. Reprints and permissions information is available online at www.nature.com/reprints. Correspondence and requests for materials should be addressed to W.K.

Competing financial interests

The authors declare no competing financial interests.

Methods

We use a combination of SIMFIRE¹⁴ and the Lund–Potsdam–Jena General Ecosystems Simulator (LPJ-GUESS), a global-scale dynamic land ecosystem and biogeochemical model¹⁶. LPJ-GUESS computes establishment, growth and mortality of several plant functional types as well as the decay and combustion of living and dead plant material³². SIMFIRE has been designed for continental to global applications and does not attempt to model ignition sources and therefore does not take into account possible future changes in lightning activity. This is a principal decision on the general modelling approach¹⁴, but note that, for example, the authors of ref. 15 did not find a significant impact of lightning activity on area burned in their global study. Increasing CO₂ levels in LPJ-GUESS lead to higher leaf biomass in water-limited environments, in accordance with satellite-based evidence²⁶, thereby increasing predicted burned area through SIMFIRE. Changes in leaf tissue carbon and nutrient status due to higher CO₂ are not included, even though these have been observed to lead to changes in leaf litter flammability³³. Even though fire numbers and size distribution^{31,34} as well as the intra-annual timing³⁵ of wildfires are influenced strongly by humans in multiple complex patterns, in particular at regional scales, most large-scale evidence shows declining burned area with increasing human presence^{11–15}. SIMFIRE uses population density as a general representation of human impact, and biome type to represent different levels of flammability leading to corresponding levels of burned area. The validity of the derived relationship, including the degree to which humans control flammability, is assumed to be invariant with time.

Fractional burned area per year (fire frequency) is computed as:

$$A(y) = a(B)F^b N_{\max}(y)^c \exp(-ep) \quad (1)$$

where y is the fire year¹⁴, B is the biome type (based on vegetation type and height), F is the interannual average of annual maximum of monthly FAPAR (fraction of absorbed photosynthetically active radiation, a measure of vegetation continuity and leaf area), N_{\max} is the annual maximum Nesterov index, and p is the population density (people km⁻²). b , c and e are global parameters, and $a(B)$ denotes one parameter a for each of eight biome types. The particular form of equation (1) and the parameter values $a(B)$, b , c and e are taken from SIMFIRE optimized against global GFED3 burned area³⁶ for the complete range of population densities¹⁴ (Supplementary Table 2). Annual fire frequency is redistributed to monthly values using the mean 2001–2010 GFED3 annual cycle of burned area within a varying radius around the grid cell centre. To determine an adequate averaging radius for each grid cell, we set its value to 250 km and compute the cumulative observed burned area for the observation period within the circle. If the cumulative observed burned area is less than 10,000 km², we increase the averaging radius until a value of 10,000 km² is reached. Grid cells that are assigned more than 50% cropland any time during 1901–2100 based on historical, RCP8.5 or RCP6.0 scenarios³⁷ are excluded in accordance with ref. 14 and to avoid the introduction of temporal trends through the use of a time-varying crop mask. We use the Nesterov index as a convenient nonlinear combination of weather variables to derive a suitable dependent variable for equation (1). We do not account for the possible impact of large-scale shifts in wind patterns, partly because wind speed from a global climate model is not identical to the top-of-canopy wind speed that is relevant for fuel drying and spread, and partly because wind speed is more important for extreme fire events³⁸ than for predicting average conditions. Our approach also reflects the caution expressed in ref. 39 about an uncritical use of wind speed in global-scale fire models.

Data. LPJ-GUESS is driven by monthly mean precipitation, temperature and radiation from the fifth phase of the Coupled Model Intercomparison Project (CMIP5) series of climate experiments⁴⁰ based on eight Earth system models (ESMs, see Supplementary Table 1), each following either RCP4.5 with moderate emissions, or RCP8.5 with high emissions²⁵. The monthly data were bias corrected on the basis of 1961–1990 mean CRU TS3.10 climatology⁴¹ and redistributed to daily values using the method of ref. 16, except for diurnal temperature range, T_r , and fraction of wet days, f_w , and the following: if monthly precipitation is <5 mm, bias correction is additive, not multiplicative.

T_r , and f_w , needed to generate daily precipitation, were derived using a stochastic model:

$$T_r(y, m) = a_T(m) + b_T(m)T_{\text{corr}}(y, m) + r_T(m)\xi \quad (2)$$

where a_T , b_T and r_T are the offset, slope and standard deviation of the residual of a linear regression between monthly mean diurnal temperature range and diurnal mean temperature derived from CRU TS3.10⁴¹ for the climatological reference period (1961–1990), and ξ is a normally distributed random number with mean 0 and standard deviation 1. The analogous formulation for f_w is:

$$f_w(y, m) = a_w(m) + b_w(m)P_{\text{corr}}(y, m) + r_w(m)\xi \quad (3)$$

where the linear regression is between number of wet days and monthly mean precipitation. Both T_r and f_w are constrained to values greater than or equal to 0.

m stands for month and y for calendar year, and T_{corr} and P_{corr} are diurnal mean temperature and precipitation, respectively, from CMIP5 after applying bias correction. If the standard deviation of any input data for the regression analysis is less than 0.1, we use diurnal temperature range or wet days derived from the CRU climatology. We use an equal-area grid with a resolution of $1^\circ \times 1^\circ$ at the Equator, but with increasing east–west spacing towards the poles.

Model coupling and parameterization. Whereas LPJ-GUESS requires fire frequency for each grid cell from SIMFIRE, SIMFIRE requires FAPAR, vegetation type and height and N_{\max} (see equation (1)) from LPJ-GUESS. N_{\max} used by SIMFIRE is computed on the basis of daily precipitation, maximum and minimum temperatures generated by LPJ-GUESS according to ref. 14, multiplied by a correction factor. This factor is computed as the ratio between the mean annual maximum Nesterov index derived from daily WATCH data⁴² during 1901–2001 divided by the generated N_{\max} averaged over the same years. The generated N_{\max} is computed as the average over 100 realizations of the weather generator used by LPJ-GUESS, but derived from monthly means of the same WATCH data. In most areas where fires occur, the ratio is 0.7–1, and close to 1 in the most fire-prone areas (see Supplementary Fig. 9).

As SIMFIRE is parameterized using remotely sensed not modelled FAPAR, coupling of SIMFIRE and LPJ-GUESS requires a procedure of bias correction. To derive the bias-correction function for FAPAR, annual potential FAPAR is simulated by LPJ-GUESS run on a global 0.5 by 0.5° grid and driven by observed burned area^{32,36}. This potential FAPAR simulated in LPJ-GUESS, which would occur at full leaf development, averaged over all individuals of each patch for the years 1998–2009, is compared with the average annual maximum satellite-derived FAPAR (based on monthly values of each year) for the same years, using SeaWiFS until 2002 and MERIS thereafter^{14,43}. As LPJ-GUESS simulates natural vegetation, the procedure uses only grid cells with less than 10% crop fraction⁴⁴ (data for 2007). We have derived three bias-correction functions, all returning a satellite FAPAR of 0 for model FAPAR of 0 by design. The results with root-mean-squared deviation (r.m.s.) and explained variance (R^2) are:

$$\text{FAPAR}_{\text{sat}} = 0.54 \text{ FPAR}_{\text{leafon}} \quad (\text{r.m.s. } 0.16, R^2 = 0.47)$$

$$\text{FAPAR}_{\text{sat}} = 0.43 \text{ FPAR}_{\text{leafon}} + 0.15 \text{ FPAR}_{\text{leafon}}^2 \quad (\text{r.m.s. } 0.16, R^2 = 0.49),$$

$$\text{FAPAR}_{\text{sat}} = 0.52 \text{ FPAR}_{\text{leafon}} - 0.14 \text{ FPAR}_{\text{leafon}}^2 + 0.21 \text{ FPAR}_{\text{model}}^3$$

$$(\text{r.m.s. } 0.16, R^2 = 0.49)$$

For lack of further improvement of the fit for the cubic function, the quadratic bias-correction function was chosen.

The optimal parameters used for SIMFIRE together with the rules used to assign the land-cover class are explained by Supplementary Table 2. The thresholds of 0.1, 0.4 and 0.6 as well as the 2 m limit for shrubs correspond to the IGBP land use definitions used to derive the land-cover classes according to ref. 45, which were also used as input data when the SIMFIRE parameters were optimized¹⁴. The criteria, however, are rather vague about what constitutes an area dominated by trees or shrub. The threshold of 0.8 for this case has been introduced to account for a substantial fraction of re-growing trees in forests without classifying the areas as shrubland. We further used a running average of simulated FAPAR over 10 years up to the current simulation year to derive F in equation (1), and the most common simulated biome type derived from each year's FPAR_leafon during the same ten-year moving time window to determine a grid cell's simulated biome.

Socio-economic scenarios. The demographic projection data are adopted from the Shared Socio-economic Pathways (SSPs)—a framework developed by the climate research community to represent plausible trends in the evolution of social and natural systems in the twenty-first century¹⁹. The SSPs include qualitative narratives and quantitative projections of the key elements of five different development pathways under which the world faces different levels of challenges to climate change mitigation and adaptation (see Supplementary Fig. 10). Among these development pathways, SSP2 reflects an intermediate case of middle of the road, with medium population growth, central urbanization and medium economic growth; SSP3 represents a fragmented world with large challenges to both mitigation and adaptation, due to rapid population growth, slow urbanization and slow economic growth. SSP5 represents a world focusing on conventional economic growth, using fossil fuels to meet high energy demand, but having slower population growth, fast urbanization, high investment in human capital and technology, which lead to high emissions and also high adaptive capacity. These three pathways were chosen to represent two extreme cases and one central case: SSP5 with low population growth and fast urbanization, SSP3 as the opposite case with high population growth and slow urbanization, and SSP2 in the middle.

We did not consider SSP1 and SSP4 because of two considerations. First, we include the RCP8.5 emissions scenario in our fire risk analysis and therefore need to consider that SSP5 is the only scenario under which integrated assessment

models can plausibly reach sufficient emissions to be consistent with RCP8.5 (see SSP Data Base Version 1.0 of May 2015, http://www.iiasa.ac.at/web/home/research/researchPrograms/Energy/SSP_Scenario_Database.html). SSP1, a sustainability pathway, has similar population growth and the same fast urbanization as SSP5, but mostly leads to low emissions and therefore is not included in our analysis. SSP4, a world of inequality, assumes high to medium population growth and fast urbanization and also leads to low emissions. We do not specifically consider SSP4, but use SSP2 medium population growth combined with fast urbanization, which reflects demographic trends similar to those of SSP4.

Simulations. LPJ-GUESS is driven by monthly mean precipitation, temperature and radiation from the CMIP5 series of climate experiments⁴⁰ based on eight ESMs (see Supplementary Information), each following either RCP4.5 with moderate emissions, or RCP8.5 with high emissions²⁵. The coupled model LPJ-GUESS–SIMFIRE has been shown to reproduce observed spatial patterns and temporal trends of burned area for Europe overall and for the Mediterranean region in particular⁴⁶.

For each combination of RCP and ESM, we run one LPJ-GUESS simulation with population density and atmospheric CO₂ fixed at the values for the year 2000, one simulation with only population density fixed at 2000, and five simulations with time-varying CO₂ according to the particular RCP, but with differing demography scenarios. For 1900 to 2005, all population scenarios use gridded population data from HYDE, which are based on the assumed location where people carry out their normal daily activities, rather than their place of residence⁴⁷. After 2005 and until 2100, we use a combination of per-country total population with per-country urbanization projections according to SSP2, SSP3 and SSP5. We also include combinations of the central estimate of SSP2 population growth with slow urbanization assumed under SSP3, or with fast urbanization following SSP5. We produce future gridded population by re-scaling urban and rural population of each country separately by their respective relative growth since 2005 based on the SSP per-country scenarios of population and urbanization, thereafter re-scaling all grid cells of a given country to match the respective SSP population scenario. Although this proportional scaling approach is the most commonly used method, it assumes no change in the pattern of the rural–urban population distribution, something that could be improved in future analyses. Processing is carried out at a spatial resolution of 0.5 by 0.5° before transforming to the LPJ-GUESS grid.

Sensitivity analysis. Two sets of sensitivity experiments are added, either with SIMFIRE optimized against a different burned-area data set⁴⁸ (MCD45, parameterization for all population densities as described in ref. 14), or with the SIMFIRE function for the impact of population density modified to reflect the possibility of a slight increase in fire frequency with population density at very low levels. Such a modification is done by multiplying $A(y)$ in equation (1) by a factor of $0.81 + 0.19 p / 0.1$, whenever p is below 0.1. This experiment considers the possibility that the fire regime in sparsely populated areas might be ignition limited^{10,14}. The simulations use output from MPI-ESM-LR for both RCP4.5 and RCP8.5 (see Supplementary Table 1).

The runs with modified population impact yield a global burned area of approximately 0.2 million km² yr⁻¹ lower on average during 1901–1930, 1971–2000, and 2071–2100 for both RCPs, producing only a small offset of global burned area that varies little across time (see Supplementary Table 5). There is a very slight impact on burned area in densely populated areas due to lasting effects on vegetation dynamics when grid cells transition from sparse to densely populated during the simulation period. The simulations using SIMFIRE parameterized against MCD45 burned area also produce a very small negative offset in global burned area for past periods, and a small positive offset for 2071–2100, with a

slightly larger temporal trend. There is also a slightly larger temporal trend in the number of people living in fire-prone areas compared with the standard SIMFIRE parameterization. The biggest impact is found for total burned area in densely populated areas, where the MCD45 parameterization systematically produces values higher by about one-quarter for 1971–2000 as well as 2071–2000 compared with the standard case. As a result, the relative change between these periods is approximately the same as for the standard case.

References

- Knorr, W., Lehsten, V. & Arneth, A. Determinants and predictability of global wildfire emissions. *Atmos. Chem. Phys.* **12**, 6845–6861 (2012).
- Manea, A., Grootemaat, S. & Leishman, M. R. Leaf flammability and fuel load increase under elevated CO₂ levels in a model grassland. *Int. J. Wildland Fire* **24**, 819–827 (2015).
- Syphard, A. D., Radeloff, V. C., Hawbaker, T. J. & Stewart, S. I. Conservation threats due to human-caused increases in fire frequency in mediterranean-climate ecosystems. *Conserv. Biol.* **23**, 758–769 (2009).
- Saarnak, C. F. A shift from natural to human-driven fire regime: implications for trace-gas emissions. *Holocene* **11**, 373–375 (2001).
- Giglio, L. *et al.* Assessing variability and long-term trends in burned area by merging multiple satellite fire products. *Biogeosciences* **7**, 1171–1186 (2010).
- Hurt, G. C. *et al.* Harmonization of land-use scenarios for the period 1500–2100: 600 years of global gridded annual land-use transitions, wood harvest, and resulting secondary lands. *Climatic Change* **109**, 117–161 (2011).
- Moritz, M. A., Moody, T. J., Krawchuk, M. A., Hughes, M. & Hall, A. Spatial variation in extreme winds predicts large wildfire locations in chaparral ecosystems. *Geophys. Res. Lett.* **37**, L04801 (2010).
- Lasslop, G., Hantson, S. & Kloster, S. Influence of wind speed on the global variability of burned fraction: a global fire model's perspective. *Int. J. Wildland Fire* **24**, 989–1000 (2015).
- Taylor, K. E., Stouffer, R. J. & Meehl, G. A. An overview of CMIP5 and the experiment design. *Bull. Am. Meteorol. Soc.* **93**, 485–498 (2012).
- Harris, I., Jones, P. D., Osborn, T. J. & Lister, D. H. Updated high-resolution grids of monthly climatic observations—the CRU TS3.10 Dataset. *Int. J. Climatol.* **34**, 623–642 (2014).
- Weedon, G. P. *et al.* Creation of the WATCH forcing data and its use to assess global and regional reference crop evaporation over land during the twentieth century. *J. Hydrometeorol.* **12**, 823–848 (2011).
- Gobron, N., Belward, A., Pinty, B. & Knorr, W. Monitoring biosphere vegetation 1998–2009. *Geophys. Res. Lett.* **37**, L15402 (2010).
- Ramankutty, N. & Foley, J. A. Estimating historical changes in global land cover: croplands from 1700 to 1992. *Glob. Biogeochem. Cycles* **13**, 997–1027 (1999).
- Friedl, M. A. *et al.* Global land cover mapping from MODIS: algorithms and early results. *Remote Sensing Environ.* **83**, 287–302 (2002).
- Wu, M. *et al.* Sensitivity of burned area in Europe to climate change, atmospheric CO₂ levels and demography: a comparison of two fire-vegetation models. *J. Geophys. Res.* **120**, 2256–2272 (2015).
- Goldewijk, K. K., Beusen, A. & Janssen, P. Long-term dynamic modeling of global population and built-up area in a spatially explicit way: HYDE 3.1. *Holocene* **20**, 565–573 (2010).
- Roy, D. P., Boschetti, L., Justice, C. O. & Ju, J. The collection 5 MODIS burned area product - Global evaluation by comparison with the MODIS active fire product. *Remote Sensing Environ.* **112**, 3690–3707 (2008).